Available online at www.sciencedirect.com
SCIENCE DIRECT
Polymer 46 (2005) 2922–2932
polymer
www.elsevier.com/locate/polymer

Analysis of an industrial continuous slurry reactor for ethylene–butene copolymerization ☆

Cristiano H. Fontes[a,*], Mario J Mendes[b,1]

[a]Departamento de Engenharia Química, Escola Politécnica, Universidade Federal da Bahia Rua Aristides Novis, 2, Federação, Salvador-Ba, Brasil
[b]Departamento de Engenharia de Sistemas Químicos, Faculdade de Engenharia Química, Universidade Estadual de Campinas, Cidade Universitária Zeferino Vaz,.Campinas-SP, Brasil

Received 12 November 2004; received in revised form 23 December 2004; accepted 25 January 2005
Available online 10 March 2005

Abstract

This work presents the analysis of a slurry polymerization stirred tank reactor for the production of high-density polyethylene. A coordination mechanism is adopted including initiation, propagation, first order deactivation, hydrogen transfer, ethylene transfer, transfer to co-catalyst and β-hydride elimination. Two site types are considered each one with its own kinetic constants. A non-uniform solid phase is considered and in the particle there is a radial distribution of chemical species such as the living and dead polymer chains. In this sense, a general local balance is proposed, providing state equations for the moments of chain length distribution and for the active site concentrations that are treated together with all others modeling scales. The multigrain model approach was adopted, combined with a simulation strategy applying orthogonal collocation. The simulation procedure handles all the equations simultaneously and the model is capable of predicting the behavior of operation variables and variables associated with the polymer properties.

Keywords: Olefin polymerization; Multigrain model; General local balance

1. Introduction

Continuous slurry polymerization with heterogeneous Ziegler–Natta catalysts is one of the most employed processes for the production of polyolefins. On the other hand, continuous polymerization processes are good candidates for MPC (Model Predictive Control) because they are multivariable, have some unusual dynamics and have more manipulated variables than controlled ones (Schnelle and Rollins [1], Moudgalya and Jaguste [24], Qin and Badgwell [25]). MPC optimizes, over the manipulated inputs, forecasts of process behavior. The forecasting is accomplished with a process model, and therefore, the model is the essential element of a MPC controller (Rawlings [2]). The objective of this work is the development of a phenomenological dynamic model of an industrial continuous slurry tank reactor for the production of high-density polyethylene through copolymerization of ethylene-1-butene with a Ziegler–Natta catalyst. Such phenomenological models, based on first principles, are naturally of a prohibitive dimension to be used in the frame of a NMPC controller for the reactor. However, aside from their eventual academic value, they can find other important uses, like that of training plant operating staff, or playing the role of the 'process' in evaluating the applicability of current advanced control tools (Schnelle and Rollins [1], Ozkan et al., [26]).

The analysis of slurry polymerization reactors is a relatively well-explored field (Ray [3], Kiparissides [4], Dube et al., [5]). In solid-catalyzed polymerizations, polymer grows at the active sites on the catalyst until chain transfer occurs, forming 'dead' polymer chains. In most cases the particle remains intact so that a single polymer particle is grown, or 'replicated', from each

Abbreviations: NAMW, number-average molecular weight; WAMW, weight-average molecular weight; ODE, Ordinary differential equation.

☆ This paper was presented in a simplified form at the II Congresso de Engenharia de Processos do Mercosul (ENPROMER'99) August 30–September 02 1999, Florianópolis, Brazil.

* Corresponding author. Tel.: 55 71 203 9801; fax: +55 71 203 9802.
E-mail addresses: cfontes@ufba.br (C.H. Fontes), mendes@desq.feq.unicamp.br (M.J. Mendes).
[1] Tel.: 13081 70, (55) (19) 3788-3941, fax: (55) (19) 3788 3910.

0032-3861/$ - see front matter © 2005 Elsevier Ltd. All rights reserved.
doi:10.1016/j.polymer.2005.01.091

Nomenclature

a_p	specific surface area of the macroparticle (cm^2/g)
$\boldsymbol{A}$, $\boldsymbol{B}$	matrices for account the derivatives of the node orthogonal polynomial at the interpolation points
c_i	concentration of species i in the macroparticle, mol/L
c_{si}	concentration of species i in the microparticle, mol/L
c_{ik}	concentration of specie i in the k collocation point, mol/L
Cd	deactivated site
$D(n, m)$	dead polymer chains with n monomer units and m comonomer units, and their concentration, mol/L
F_i	feed flow rate of component i, kg/h
K_i	mass transfer coefficient of component i, cm/min
k_p	rate of propagation constants, L/(mol·min)
$k_{t,s}$	rate constant for β-hydride elimination, min^{-1}
k_t	other rate constants for chain transfer, 1/(mol·min)
k_d	rate constant for deactivation, min^{-1}
m_i^g	mass of component i in the reactor headspace, ton
m_i^l	mass of component i in the reactor liquid phase, ton
m_i^s	mass of component i in the reactor solid phase, ton
m_i^t	total mass of component i in the reactor, ton
m_p	total mass of polymer inside the reactor, ton
n_i^g	moles of component i in reactor gas had-space
NCL	number of internal collocation points
$P_1(n, m)$	living polymer chains with n monomer units and m comonomer units, with terminal monomer, and their concentration, mol/(L_{catal})
$P_2(n, m)$	living polymer chains with n monomer units and m comonomer units, with terminal comonomer, and their concentration, mol/(L_{catal})
P_r	reactor pressure, kgf/cm^2
$P(0,0)$, $P_{0,0}$	concentration of active sites, mol/(L_{catal})
P_{NX}^s	vapor pressure of solvent, kgf/cm^2
q	volumetric flow of slurry, m^3/h
r	radial position in growing polymeric particle, cm
r_s	radial position in the growing microparticle, cm
R	radius of macroparticle, cm
R_0	initial radius of macroparticle, cm
R_c	radius of catalyst fragment, cm
R_s	radius of microparticle, cm
R_i	rate of production of species i per unit volume of catalyst, mol/(L_{catal} min)
R_{vi}	rate of production of species i per unit volume of macroparticle, mol/(L_{catal} min)
$\bar{R}_i$	mean rate of production of species i per unit mass of polymer in macroparticle, mol g^{-1} min^{-1}
R_{pol}	production rate, ton/min
$R_{p_j(0,0)}$	rate of active sites of type j
T_r	reactor temperature, °C
Te	temperature of feed stream, °C;
t	time
V_g	volume of gas head-space in reactor, m^3
V_l	volume of liquid phase in slurry, m^3
V_s	volume of solid phase in slurry, m^3
V_{sl}	volume of slurry inside the reactor, m^3
V_c	catalyst volume inside reactor, L
$\dot{V}_{cs}$	volumetric flow of catalyst withdrawal, L/min
$\dot{V}_{ce}$	volumetric flow of catalyst feed stream, L/min
w_1	monomer molecular weight
w_2	comonomer molecular weight
x	mass fraction of component i in the liquid phase
y	mass fraction of component i in the gas head-space
$\Delta H_{R,pol}$	heat of polymerization, kJ/kg
η	sorption factor
ρ	density

Subscripts:

p	polymer
i	specie or component
j	site type

Superscripts:

o	catalyst feed stream
j	site type

catalyst particle. Commercially produced polyolefins have polydispersities ranging from 3 to 20, while from theory for standard olefin polymerization kinetics an ultimate polydispersity of 2 is predicted. The broad MWD (Molecular Weight Distribution) in olefin polymers is attributed, on one hand, to monomer diffusion resistance in the growing polymer particle; on the other hand, this broad MWD has also been linked to catalytic site heterogeneity (Soares and Hamielec [6], Floyd et al. [7], Mckenna and Soares [8]. In this way, an efficient model of a slurry polymerization reactor should include the transport in the polymer phase and the heterogeneity of the catalytic sites.

Fig. 1 represents schematically the reactor. Ethylene, 1-butene (comonomer) and hydrogen (chain transfer agent), together with *n*-hexane (solvent), Ziegler– Natta type catalyst and co-catalyst are fed continuously to the reactor, while the solid–liquid slurry, present in the reactor together with a gas phase, is continuously removed from the reactor.

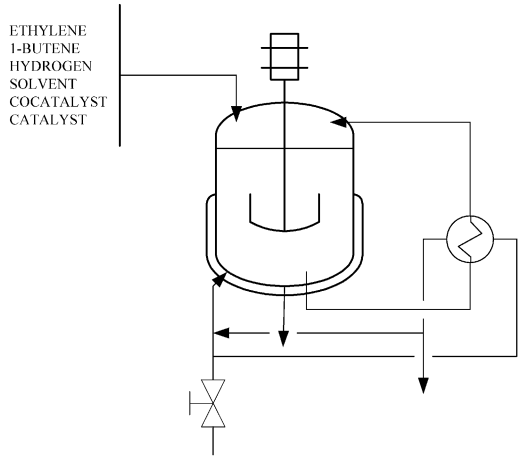

Fig. 1. Schematic representation of the reactor.

For the control of the reactor temperature, heat is exchanged in the reactor jacket and by circulation of the solid–liquid slurry through external heat exchangers.

The analysis of a simple chemical reactor considers normally three main hierarchical levels (Aris [9]). These levels are naturally found in the analysis of a slurry polymerization reactor, as shown in Table 1.

The understanding and description of the phenomena at each one of these levels and of the connections between the levels leads to the model of the reactor.

2. Kinetics of heterogeneous Ziegler–Natta polymerization

Ziegler–Natta catalysts are anionic coordination catalysts (Kiparissides [4]) (Table 2).

For heterogeneous Ziegler–Natta catalysis, even on the same catalyst particle, different active sites can have different propagation rate constants, which as seen above can give rise to very broad molecular weight distributions. Two types of catalytic sites are considered in this work (Table 2). Implicit in the kinetic equations is the concept of the terminal model for copolymerization (Soares and Hamielec [6]). The absence of a site activation step in the proposed mechanism is explained by the assumption of the existence of a prepolymerization operational stage before the reactor feeding. This assumption is related to the cocatalyst effect on the dynamic behavior of reactor.

According to the mechanism of Table 2 and using the global constants

$$k_{t,ghj} = k_{t,sj} + k_{t,h_j} C_{sH_2}, \tag{1a}$$

$$k_{t,cce_j} = k_{t,cc_j} C_{sCC} + k_{t,me_j} C_{sET}, \tag{1b}$$

$$k_{t,ccb_j} = k_{t,cc_j} C_{sCC} + k_{t,mb_j} C_{sET}, \tag{1c}$$

the rate of production of the living chains P_{1j} (n,m) per unit volume of catalyst is:

$$\begin{aligned} R_{P_{ij}(n,m)} = &-\left[k_{t,hgj} + k_{p,eej} C_{sET} + k_{p,ebj} C_{sBT} + k_{t,ccej} \right. \\ &\left. + k_{d,j}\right] P_{1j}(n,m) + k_{p,eej} C_{sET} P_{1j}(n-1,m) \\ &+ k_{p,bej} C_{sET} P_{2j}(n-1,m) \quad (\geq 1, m \geq 1) \end{aligned} \tag{2}$$

For well-known reasons (Ray [10], Hutchinson et al. [11]), the state of the polymer was represented mathematically using the method of moments, so that the model obtained provides only the prediction of average polymer properties. The (ik) th moments of living (growing) chains ended with monomer or comonomer at site type j are

$$\lambda_{1_j}^{ik} = \sum_{n=1}^{\infty} \sum_{m=0}^{\infty} n^i m^k P_{1_j}(n,m) \tag{3a}$$

and

$$\lambda_{2_j}^{ik} = \sum_{n=0}^{\infty} \sum_{m=1}^{\infty} n^i m^k P_{2_j}(n,m) \tag{3b}$$

respectively, while

$$\Lambda^{ik} = \sum_{n=0}^{\infty} \sum_{m=0}^{\infty} n^i m^k D(n,m) \tag{3c}$$

is the (ik)th moment of the dead chains. Rate equations for the zero, first and second order moments for each active site type $(\lambda_{1_j}^{00}, \lambda_{2_j}^{00}, \Lambda_j^{00}, \lambda_{1_j}^{10}, \lambda_{2_j}^{10}, \Lambda_j^{10}, \lambda_{1_j}^{01}, \lambda_{2_j}^{01}, \Lambda_j^{01}, \lambda_{1_j}^{11}, \lambda_{2_j}^{11}, \Lambda_j^{11}, \lambda_{1_j}^{20}, \lambda_{2_j}^{20}, \Lambda_j^{20}, \lambda_{1_j}^{02}, \lambda_{2_j}^{02}$ and Λ_j^{02} are obtained from the balances of living and dead chains and from definitions (Eqs. (3a–c)). Thus, for example, the rate of production per unit volume of catalyst of the zero order moment $\lambda_{1_j}^{00}$ is given by (Fontes [12]):

$$\begin{aligned} R_{\lambda_{1j}^{00}} = &-(k_{d,j} + k_{p,ebj} C_{sBT} + k_{t,hgi}) \lambda_{1_j}^{00} \\ &+ k_{p,eej} C_{sET} P_j(0,0) + k_{p,bej} C_{sET} \lambda_{2j}^{00} + k_{t,ccbj} \lambda_{2_j}^{00} \end{aligned} \tag{4}$$

For each site type there are thus 18 rate equations for the moments of zero, first and second order. On the other hand, the production rates per unit volume of catalyst of ethylene, 1-butene and hydrogen, at each type of active site j, are given by:

Table 1
Hierarchical scales of the analysis of a slurry polymerization reactor (Ray [3])

1. Microscale: Polymerization kinetics; Nature of active sites;
2. Mesoscale: Inter- and intraphase heat and mass transfer;
3. Macroscale: Overall material and energy balances; Macromixing.

Table 2
The kinetic mechanism of copolymerization

Site type $j(j=1,2)$

$$
\begin{cases}
-\text{Initiation}: \\
P_j(0,0)+\text{ET} \longrightarrow^{k_{p,eej}} P_{1_j}(1,0) \\
P_j(0,0)+\text{BT} \longrightarrow^{k_{p,bbj}} P_{2_j}(0,1) \\
-\text{Propagation}: \\
P_1(n,m)+\text{ET} \longrightarrow^{k_{p,eej}} P_{1_j}(n+1,m) \\
P_2(n,m)+\text{ET} \longrightarrow^{k_{p,bej}} P_{1_j}(n+1,m) \\
P_1(n,m)+\text{BT} \longrightarrow^{k_{p,ebj}} P_{2_j}(n,m+1) \\
P_2(n,m)+\text{BT} \longrightarrow^{k_{p,bbj}} P_{2_j}(n,m+1)
\end{cases}
\qquad
\begin{cases}
-\text{Chain Transfer}: \\
P_{1_j}(n,m) \longrightarrow^{k_{t,sj}} P_j(0,0)+D_j(n,m) \\
P_{2_j}(n,m) \longrightarrow^{k_{t,sj}} P_j(0,0)+D_j(n,m) \\
P_{1_j}(n,m)+\text{H}_2 \longrightarrow^{k_{t,hj}} P_j(0,0)+D_j(n,m) \\
P_{2_j}(n,m)+\text{H}_2 \longrightarrow^{k_{t,sj}} P_j(0,0)+D_j(n,m) \\
P_{1_j}(n,m)+\text{ET} \longrightarrow^{k_{t,mej}} P_1(1,0)+D_j(n,m) \\
P_{2_j}(n,m)+\text{ET} \longrightarrow^{k_{t,mbj}} P_1(1,0)+D_j(n,m) \\
P_{1_j}(n,m)+\text{CC} \longrightarrow^{k_{t,ccj}} P_1(1,0)+D_j(n,m) \\
P_{2_j}(n,m)+\text{CC} \longrightarrow^{k_{ccj}} P_{1j}(1,0)+D_j(n,m) \\
-\text{Deactivation}: \\
P_{1_j}(n,m) \longrightarrow^{k_{d,j}} Cd_j+D_j(n,m) \\
P_{2_j}(n,m) \longrightarrow^{k_{d,j}} Cd_j+D_j(n,m)
\end{cases}
$$

$$R_{\text{ET}j} = -[k_{\text{p},eej}(\lambda_{1j}^{00}+P_j(0,0))+k_{\text{t},mej}\lambda_{1j}^{00}+k_{\text{p},bej}\lambda_{2j}^{00} + k_{\text{t},mbj}\lambda_{2j}^{00}]C_{\text{sET}}, \tag{5}$$

$$R_{\text{BT}j} = -\left\lfloor k_{\text{p},bbj}(\lambda_{2j}^{00}+P_j(0,0))+k_{\text{p},ebj}\lambda_{1j}^{00}\right\rfloor C_{\text{sBT}}, \tag{6}$$

$$R_{\text{H}_2j} = -\left\lfloor k_{\text{t},hj}(\lambda_{2j}^{00}+\lambda_{1_j}^{00})\right\rfloor C_{\text{sH2}}, \tag{7}$$

while the rate of production of each active site is:

$$R_{\text{P}_j(0,0)} = -(k_{\text{p},eej}C_{\text{sET}}+k_{\text{p},bbj}C_{\text{sBT}}+k_{\text{d},j})P_j(0,0) + k_{\text{t},hgj}(\lambda_{1j}^{00}+\lambda_{2j}^{00}). \tag{8}$$

Considering the existence of two types of monomer units and of two site types, one obtains finally for the number-average molecular weight ($NAMW=M_{\text{n}}$), for the weight-average molecular weight ($WAMW=M_{\text{w}}$), and for the fraction of comonomer incorporated into the polymer (X_{BT}):

$$M_{\text{n}} = w_1\frac{\sum_{j=1}^{2}\lambda_j^{10}}{\sum_{j=1}^{2}\lambda_j^{00}}+w_2\frac{\sum_{j=1}^{2}\lambda_j^{01}}{\sum_{j=1}^{2}\lambda_j^{00}}, \tag{9}$$

$$M_{\text{w}} = \frac{\sum_{j=1}^{2}(w_1^2\lambda_j^{20}+2w_1w_2\lambda_j^{11}+w_2^2\lambda_j^{02})}{\sum_{j=1}^{2}(w_1\lambda_j^{10}+w_2\lambda_j^{01})}, \tag{10}$$

$$X_{\text{BT}} = \frac{\sum_{j=1}^{2}\lambda_j^{01}}{\sum_{j=1}^{2}(\lambda_j^{01}+\lambda_j^{10})} \tag{11}$$

with $\lambda_j^{ik}=\lambda_{1j}^{ik}+\lambda_{2j}^{ik}+\Lambda_j^{ik}$. The polydispersity index I_{p} is calculated directly from M_{w} and M_{n} (Hutchinson [11])

$$I_{\text{p}} = \frac{M_{\text{w}}}{M_{\text{n}}}. \tag{12}$$

Thus, not only the rates of production of the chemical components but also the important mean properties of the copolymer can be expressed as functions of the moments of zero, first and second order.

3. Transport with reaction in the polymer particles

As mentioned above, it is generally assumed that both phenomena, namely multiplicity of active site types and mass and heat transfer within the polymer particle, might play a role in the broadening of the MWD of polymers produced with supported Ziegler–Natta catalysts. From the several types of models that include inter- and intraparticle transport (Dube et al. [5], Mckenna and Soares [8]), the multigrain model (Mckenna and Soares [8], Sun et al. [21]), schematically represented in Fig. 2, was used in the present work.

This model considers the complete rupture of the catalyst at time zero, leading to the existence of two different levels for transport, the macro and microparticle levels. It will be assumed that the intraparticle temperature gradients are

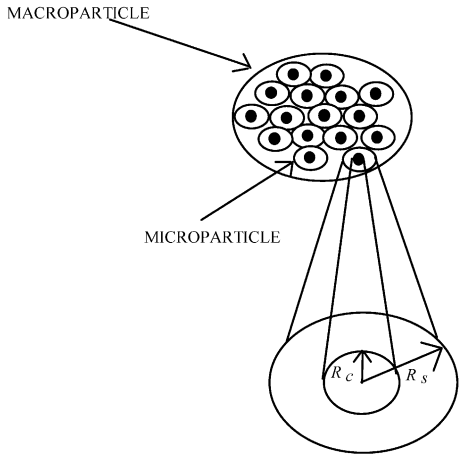

Fig. 2. Multigrain approach for the particle growth.

negligible (Mckenna and Soares [8]). Neglecting the convective mass transfer inside the macroparticle and the instantaneous variation of its volume, a global material balance for component i (i=ET, BT, H_2) on the macroparticle leads to the equations

$$\frac{\partial c_i}{\partial t} = \frac{2}{r} D_{\mathrm{eff},i} \frac{\partial c_i}{\partial r} + D_{\mathrm{eff},i} \frac{\partial^2 c_i}{\partial r^2} - R_{\mathrm{v}i}. \tag{13}$$

Eq. (13) are solved with the following initial and boundary conditions:

$$r = 0: \ \frac{\partial c_i}{\partial r} = 0, \tag{13a}$$

$$r = R(t): \ D_{\mathrm{eff},i} \frac{\partial c_i}{\partial r} = K_i [c_i^l - c_i(R,t)], \tag{13b}$$

$$t = 0: \ c_i(r,0) = c_{i0}. \tag{13c}$$

$D_{\mathrm{eff},i}$ is the effective diffusivity of species i in the macroparticle. $R_{\mathrm{v}i}$, the rate of production of species i per unit volume of the macroparticle, is related with R_i, the total rate of production of i per unit volume of catalyst (Eqs. (5)–(7)).

$$R_i = \sum_{j=1}^{2} R_{ij} \tag{14}$$

and

$$R_{\mathrm{v}i} = \frac{(1-\varepsilon) R_i}{\phi^3}. \tag{15}$$

ε is the macroparticle porosity, which will be assumed to be uniform and constant in the macroparticle, and ϕ is the microparticle growth factor (Eq. 18). Monomer, which diffuses through the macroparticle pores, adsorbs on the layer of polymer surrounding the catalyst fragments, and diffuses through this layer to the active sites on the surface of those fragments.

The mass balance equations for the microparticle are then:

$$\frac{\partial c_{\mathrm{s}i}}{\partial t} = D_{\mathrm{s}i} \frac{1}{r_{\mathrm{s}}^2} \frac{\partial}{\partial r_{\mathrm{s}}} \left(r_{\mathrm{s}}^2 \frac{\partial c_{\mathrm{s}i}}{\partial r_{\mathrm{s}}} \right), \tag{16}$$

with

$$r_{\mathrm{s}} = R_{\mathrm{s}}(t): \ c_{\mathrm{s}i} = \eta_i c_i, \tag{16a}$$

and

$$r_{\mathrm{s}} = R_{\mathrm{c}}: 4\pi R_{\mathrm{c}}^2 D_{\mathrm{s}i} \frac{\partial c_{\mathrm{s}i}}{\partial r_{\mathrm{s}}} = -\frac{4}{3} \pi R_{\mathrm{c}}^3 R_i. \tag{16b}$$

η_i is the sorption factor (equilibrium at the solid–liquid interface). A uniform distribution of cocatalyst is supposed to exist on the solid phase. Employing the Quasi Steady State Approximation for the material balance of the microparticle (Hutchinson [11]), one obtains for the concentration of each component at the surface of the catalyst fragment:

$$c_{\mathrm{s}i}^0 = \eta_i c_i - \frac{R_{\mathrm{c}}^2}{3 D_{\mathrm{s}i}} R_i \left(1 - \frac{1}{\phi} \right), \tag{17}$$

where the microparticle growth factor ϕ is defined by

$$\phi(r,t) = \frac{R_{\mathrm{s}}(r,t)}{R_{\mathrm{c}}} \tag{18}$$

$\phi^3(r,t)$ is thus the ratio of the total volume of the microparticle to the volume of the catalyst fragment in the microparticle at radial position r and instant t, and its value can be obtained from the moments of the chain length distribution (Fontes [12]):

$$\phi^3 = 1 + \frac{w_1 \sum_{j=1}^{2} \lambda_j^{10} + w_2 \sum_{j=1}^{2} \lambda_j^{01}}{\rho_{\mathrm{p}}} \tag{19}$$

The assumption of a non-uniform species distribution on the macroparticle, intrinsic to the multigrain model, leads to a radial variation of the moments and of the active site concentrations. These distributions are given by the equations (see Appendix):

$$\frac{\partial \lambda_1^{ik}}{\partial t} = R_{\lambda_1^{ik}} - \frac{\dot{V}_{\mathrm{ce}}}{V_{\mathrm{c}}} \lambda_1^{ik}, \tag{20}$$

$$\frac{\partial \lambda_2^{ik}}{\partial t} = R_{\lambda_2^{ik}} - \frac{\dot{V}_{\mathrm{ce}}}{V_{\mathrm{c}}} \lambda_2^{ik}, \tag{21}$$

$$\frac{\partial \Lambda_2^{ik}}{\partial t} = R_{\lambda_2^{ik}} - \frac{\dot{V}_{\mathrm{ce}}}{V_{\mathrm{c}}} \Lambda_2^{ik}, \tag{22}$$

$$\frac{\partial P_{0,0}}{\partial t} = R_{\mathrm{P}_{0,0}} + \frac{\dot{V}_{\mathrm{ce}}}{V_{\mathrm{c}}} (P_{0,0}^o - P_{0,0}), \tag{23}$$

where

$$\lambda_1^{ik}(r,t) = \sum_{j=1}^{2} \lambda_{1j}^{ik}(r,t), \lambda_2^{ik}(r,t) = \sum_{j=1}^{2} \lambda_{2j}^{ik}(r,t), \Lambda^{ik}(r,t) = \sum_{j=1}^{2} \Lambda_j^{ik}(r,t).$$

The newly formed polymer chains push the previously formed polymer layer, thus increasing the radius of the microparticles and consequently the size of the macroparticles. Let $\mathrm{d}V_{\mathrm{m}}$ be the volume of the macroparticle between r and $r+\mathrm{d}r$ and $\mathrm{d}V_{\mathrm{sd}}$ the volume of the solid (polymer+catalyst), that is, the volume of the microparticles, in $\mathrm{d}V_{\mathrm{m}}$. Then

$$\mathrm{d}V_{\mathrm{m}} = \frac{\mathrm{d}V_{\mathrm{sd}}}{(1-\varepsilon)} = 2\pi R^3 \gamma^{1/2} \mathrm{d}\gamma, \tag{24}$$

where $\gamma^{1/2} = r/R$. With the definition of the growth factor ϕ the volume of catalyst in $\mathrm{d}V_{\mathrm{m}}$ is then given by

$$dV_{cat}(\gamma,t)=\frac{dV_{sd}}{\phi^3}=2\pi R^3\frac{(1-\varepsilon)}{\phi^3}\gamma^{1/2}d\gamma,$$

or

$$V_{cat}=\frac{4}{3}(1-\varepsilon)\pi R_0^3=2\pi(1-\varepsilon)R^3\int_0^1(1/\phi^3)\gamma^{1/2}d\gamma. \quad (25)$$

Eq. (25) can be written in the form

$$\Phi_m^3=\left(\frac{R}{R_0}\right)^3=\frac{2}{3\int_0^1(1/\phi)^3\gamma^{1/2}d\gamma}, \quad (26)$$

where Φ_m is a 'global macroparticle growth factor'.

For the mean rate of production of component i per unit mass of polymer, $\bar{R}_i$, one obtains

$$\bar{R}_i(t)=\frac{\int_{V_m}R_{vi}dV_m}{\int_{V_m}[w_1(\lambda_1^{10}+\lambda_2^{10}\Lambda^{10})+w_2(\lambda_1^{01}+\lambda_2^{01}\Lambda^{01})][(1-\varepsilon)\phi^3]dV_m}, \quad (27)$$

while the specific surface area of the macroparticle is

$$a_p(t)=\frac{4\pi R^2}{\int_{V_m}[w_1(\lambda_1^{10}+\lambda_2^{10}\Lambda^{10})+w_2(\lambda_1^{01}+\lambda_2^{01}\Lambda^{01})][(1-\varepsilon)/\phi^3]dV_m}. \quad (28)$$

4. Macroscale modeling

Based on the operational practice and on information available in literature some simplifying assumptions were adopted:

(1) The reactor level (total slurry volume) is held constant.
(2) The temperature in the reactor is uniform (Floyd et al. [13], Soares and Hamielec [14]).
(3) Thermodynamic equilibrium exists at the gas–liquid interface (Floyd et al. [7], Mckenna and Soares [8]).
(4) The gas and slurry phases are well mixed.

It should be considered that the well-mixed characteristics of the phases in reactor generate a residence time distribution for the macroparticles in reactor. To capture the effects of such a distribution, population balance techniques should be used in the construction of the model of the reactor (Zacca et al. [15]). There is, however, some evidence that for sufficiently active catalysts the effect of particle size distribution might be of less importance (Galvan and Tirrel [16]).

With the above hypotheses the mass balances for component i in the liquid, gas and solid phases take the form:

$$\frac{d(m_i^g+m_i^l)}{dt}=F_i-\frac{q}{V_s+V_l}m_i^l-K_ia_p(c_i^l-c_i(R,t)), \quad (29)$$

$$\frac{dm_i^s}{dt}=-\bar{R}_im_p-\frac{q}{V_s+V_l}m_i^s-K_ia_pm_p(c_i^l-c_i(R,t). \quad (30)$$

m_i^g, m_i^l and m_i^s are the masses of component i present in the gas, liquid and solid phases of the reactor, $V_{sl}=V_s+V_l$ is the slurry volume in reactor, q is the volumetric flow rate of slurry leaving the reactor and $\bar{R}_i$ is the mean rate of production of i per unit mass of the solid present in the reactor.

Overall mass and energy balances are:

$$\frac{d\left(\sum_i m_i^g+\sum_i n_i^l+\sum_i m_i^s\right)}{dt}=\sum_i F_i-q\frac{\left(\sum_i m_i^l+\sum_i m_i^s\right)}{V_l+V_s}, \quad (31)$$

$$\sum_i m_i^tC_{pi}\frac{dT_r}{dt}=-\sum_i F_iC_{pi}(T_r-Te_i)-\dot{Q}_c-\dot{Q}_t+(-\Delta H_{R,pol})R_{pol}, \quad (32)$$

where R_{pol} is the global rate production of polymer, and $\dot{Q}_c$ and $\dot{Q}_t$ are the heat transfer rates in the reactor jacket and in the external heat exchangers, respectively.

5. Simulation

No effort has been made to identify the model parameters; typical literature values were used instead. The constant volume restriction

$$V_s+V_l=\sum_i\frac{m_i^l}{\rho_i}+\sum_i\frac{m_i^s}{\rho_i}=V_{sl}, \quad (33)$$

and the hypothesis of ideal gas behavior (Soares and Hamielec [14]),

$$P_r=\sum_i n_i^g\frac{R_gT_r}{V_g}, \quad (34)$$

provided additional algebraic equations of the model. Henry's law was used to calculate the concentration of monomer, comonomer, hydrogen and nitrogen in the liquid phase,

$$y_iP_r=h_ix_i,(i=ET,BT,H_2,N_2), \quad (35)$$

while Raoult's law was applied to the solvent (Soares and Hamielec [14]).

$$y_{NX}P_r=x_{NX}P_{NX}^s(T_r) \quad (36)$$

The Henry constants and densities as functions of temperature were obtained using available correlations (Freitas [17]). The correlation of Marrone and Kirwan [18] was used to calculate the liquid–solid mass transfer coefficients. Table 3 shows the values of the frequency factors for the rate constants (Freitas [17]).

For the activation energies of the propagation, chain transfer and deactivation steps, respectively, the values of 29.4 kcal/mol, 50.2 kJ/mol and 4.2 kJ/mol were taken.

Typical values for the macroparticle and microparticle diffusivities are shown in Table 4 (McAuley et al. [19], Mckenna et al., [20]). The macroparticle porosity ε was assumed constant and equal to 0.4 (McAuley et al. [19]). The sorption factor η_i (solid–liquid interface) was assumed to be unity.

With the exception of the equations of the multigrain model, the phenomenological model presented above is made of ordinary differential and algebraic equations. The equations of the multigrain model were integrated using the classical orthogonal collocation method (Villadsen and Michelsen [22]). Following this approach, Eq. (13) are transformed into:

$$\frac{dc_{i,k}}{dt} = \frac{6}{R^2} D_{\mathrm{eff},i} \sum_{j=1}^{\mathrm{NCL}+1} A_{kj} c_{i,j} + \frac{4\gamma_k}{R^2} D_{\mathrm{eff},i} \sum_{j=1}^{\mathrm{NCL}+1} B_{kj} c_{i,j} - R_{i,k}, (k = 1, \ldots \mathrm{NCL}), \tag{37}$$

with the boundary condition:

$$\gamma = 1 : \frac{2D_{\mathrm{eff},i}}{R} \sum_{j=1}^{\mathrm{NCL}+1} A_{\mathrm{NCL}+1,j} c_{ij} = K_i \left[c_i^{\mathrm{l}} - c_{i,\mathrm{NCL}+1} \right]. \tag{38}$$

NCL is the number of interior collocation points. Gaussian Quadrature was used to integrate equation (26) for the radius of the macroparticle.

Table 3
Frequency factors of the kinetic constants ($L.mol^{-1}.min^{-1}$)

	Site 1	Site 2
Propagation:		
$K_{p,ee}$	1.101×10^{8}	1.101×10^{8}
$K_{p,be}$	2.591×10^{6}	1.943×10^{7}
$K_{p,eb}$	8.290×10^{7}	8.290×10^{7}
$K_{p,bb}$	1.943×10^{6}	8.031×10^{6}
Chain transfer		
$K_{t,s}$ (min^{-1})	1.615×10^{5}	1.615×10^{5}
$K_{t,h}$	1.421×10^{8}	1.421×10^{7}
$K_{t,me}$	3.392×10^{6}	3.392×10^{5}
$K_{t,mb}$	3.392×10^{6}	1.615×10^{5}
$K_{t,cc}$	3.876×10^{7}	3.876×10^{6}
Deactivation		
K_d (min^{-1})	3×10^{-1}	3×10^{-1}

Table 4
Diffusivities ($cm^2\ min^{-1}$)

Species	Macroparticle D_{eff}	Microparticle D_{si}
Ethylene	1.2×10^{-4}	6×10^{-5}
1-butene	1×10^{-4}	6×10^{-5}
Hydrogen	3.6×10^{-4}	6×10^{-5}
Nitrogen	0.6×10^{-4}	–
n-hexane	1.5×10^{-4}	–

With two types of catalytic sites $36\times(\mathrm{NCL}+1)+2\times(\mathrm{NCL}+1)$ ordinary differential equations were thus obtained for the multigrain model, comprising the balances for the moments of the chain length distribution and the active sites. Table 5 incorporates all the equations of the complete dynamic model. Thus, for example, using five interior collocation points, NCL = 5, the differential algebraic equation system of the model comprises 14 algebraic equations and 267 ordinary differential equations.

A differential-algebraic system equation solver (Le Roux [23]) was employed for the simulation. Two sets of simulation tests were performed. A first set of tests was intended to evaluate the model through the response to different step changes of the feed rates of hydrogen, catalyst, comonomer, solvent (*n*-hexane) and co-catalyst. These inputs were selected due to their expected effects on the process outputs. Table 6 presents the magnitude of each input step change and the time of its application. With the exception of 1-butene (comonomer), all the imposed changes represented feasible operational changes. In normal operation conditions the feed rate of the comonomer is much lesser than that of ethylene, so that a high step change F_{BT} was imposed in order to enable the detection of its effect on the process variables and on the polymer properties.

In all simulation tests, the initial steady state was obtained using the dynamic model itself (false transient); the initial state obtained in this way was used as the basis for the data normalization. Table 7 presents the absolute initial values of all input variables together with initial values for the weight-average molecular weight (WAMW), number average molecular weight (NAMW) (output variables), and temperature (state variables), according to Figs. 3–5.

Fig. 3 presents the influence of the number of types of catalytic sites on the variation of the polydispersity due to the step input changes defined in Table 6. In both cases all the other model parameters were the same. The results of Fig. 3b showed a polydispersity index close to 2 and not too sensible to the perturbations imposed on the feed rates, while for Fig. 3a the polydispersity index was always greater than 2 and showed sensible variations with the input changes. These results show that, under the polymerization conditions assumed in this work, the effect of multiple types of catalytic sites on the polymer properties (polydispersity index) is more important than that of mass transfer resistances in the macroparticle.

Table 5
Dimension of the complete dynamic model using orthogonal collocation for the multigrain equations.

	Number of equations
Statistic moments	18×2×(NCL+1)
Active sites balances	2×(NCL+1)
Macroparticle mass balances	5×NCL
Algebraic equations	14
Component mass balances	12
Overall energy and mass balances	2
Total of equations	18×2×(NCL+1)+2×(NCL+1)+5×NCL+28

Fig. 4 presents the results for the changes of the weight-average molecular weight (WAMW) and of the number average molecular weight (NAMW) due to the input changes. The increase in hydrogen concentration led immediately to a decrease of WAMW and of NAMW, due to an intensification of hydrogen chain transfer. The model also predicted an increase in the polydispersity index due to a raise in hydrogen concentration, as expected (Fontes [12]). The effect of the comonomer feed rate on the polidispersity can be assigned to the increase in the comonomer composition and to the deviation from the homo-polymerization conditions. The small effect of the catalyst feed rate on the polydispersity index can be attributed to the simultaneous reduction in both WAMW and NAMW. The reduction in these average molecular weights due to increase in the catalyst feed rate is assigned to the raise in active site concentration. The *n*-hexane effect in the polymer properties is due to increase in temperature.

Although the ratio of propagation rate to transfer rate for 1-butene was assumed to be smaller than that for ethylene, the increase in the WAMW, due to the positive step in the comonomer feed ($t=1000$ min), is attributed to the higher molecular weight of the comonomer. In this case, an opposite effect was observed on the NAMW.

Fig. 5 shows the temperature behavior. The strong effect of the comonomer feed rate is due to the high step change imposed in this case.

Figs. 3–5 show that the response of process variables such as temperature is typically more rapid than that of the polymer properties (WAMW, NAMW, polydispersity index), confirming the high value of the time constants associated with the reactional variables. On the other hand, a relatively low effect of the cocatalyst feed rate on all output variables analyzed was observed. The inclusion of a site activation step in the kinetic model (Table 2) would have increased this effect.

Table 6
Step changes on the main input variables (simulation test).

Step input	Application instant, (min)
Hydrogen feed flow (F_{H2}) (+50%)	25
Catalyst feed flow(F_C) (+33%)	500
Comonomer feed flow (F_{BT}) (+1000%)	1000
Solvent feed flow (F_{NX}) (-19%)	1500
Cocatalyst feed flow (F_{CC}) (+250%)	2000

Table 7
Initial absolute values for simulation tests (figures 3–5, two active sites)

Hydrogen feed flow	10 kg/h
Catalyst feed flow	0.075 kg/h
Comonomer feed flow	150 kg/h
Solvent feed flow	16000 kg/h
Cocatalyst feed flow	0.2 kg/h
Monomer feed flow	7500 kg/h
Water flow in the reactor jacket	150000 kg/h
Water flow in the external heat external heat exchangers	60000 kg/h
WAMW	122000
NAMW	29017
Temperature	84.6 °C

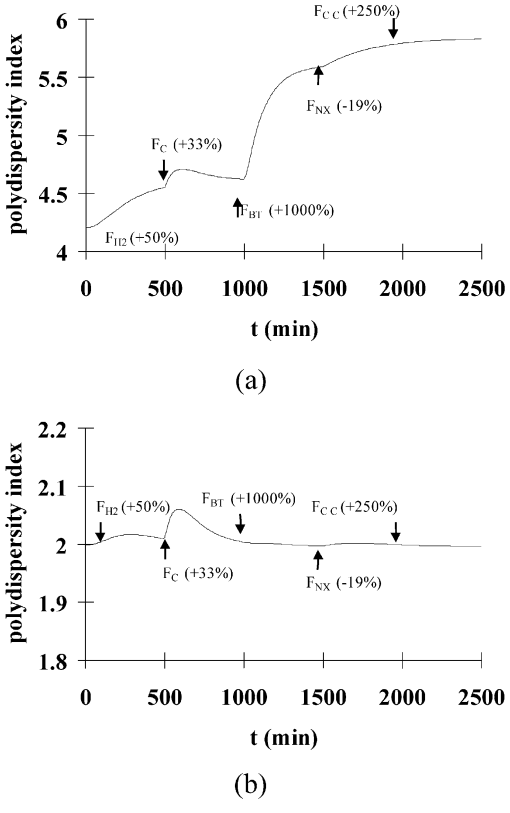

Fig. 3. Influence of the number of types of catalytic sites on the reactor dynamics (polydispersity index): (a) kinetic model with two types of catalytic sites; (b) kinetic model with one type of catalytic site.

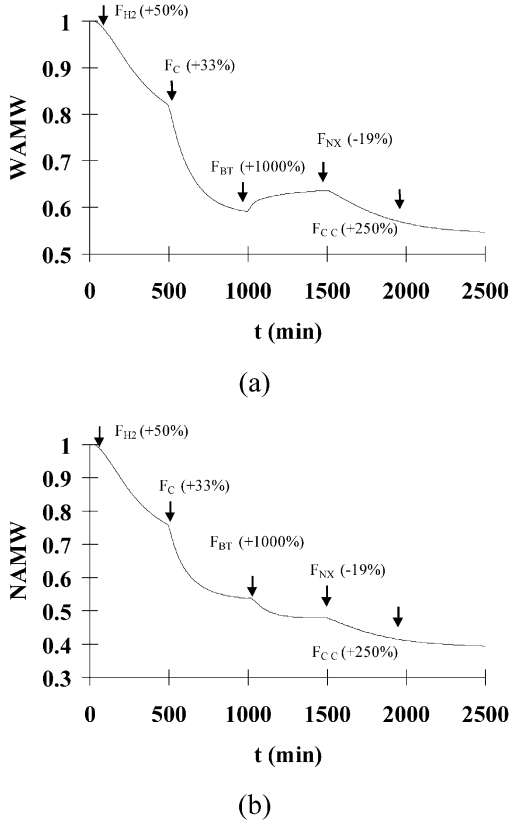

Fig. 4. Dynamic response of: (a) normalized WAMW; (b) normalized NAMW.

A second set of simulation tests was accomplished in order to evaluate the predictive character of the model, using values of the hydrogen/ethylene ratio in the reactor gas phase measured by chromatographic analysis for three distinct operational runs (Figs. 6 and 7). These data, together with the input flows, are reliably and were collected directly from the data acquisition system. Despite the noisy behavior of the plant data, the model predicts in both cases the dominant tendency of the process dynamics. Furthermore, the quality of the results shown in Figs. 6 and 7 is good indeed, considering that the data collected from the plant included no values of the hydrogen flow rate.

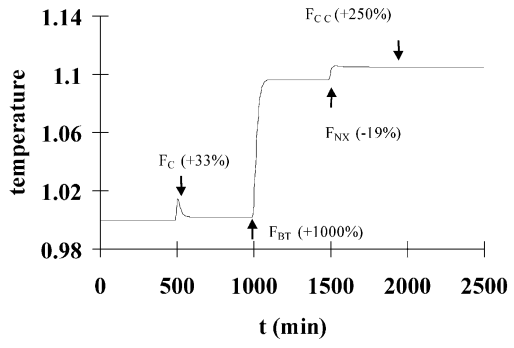

Fig. 5. Variation of the normalized reactor temperature due to input step changes.

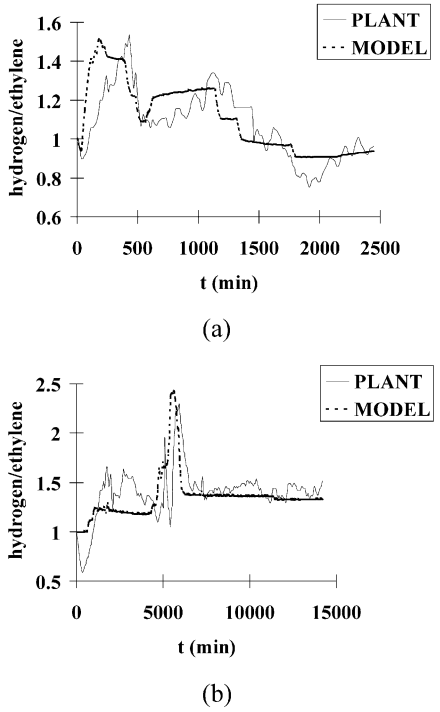

Fig. 6. Normalized hydrogen/ethylene ratio for two distinct operational runs.

The high fluctuations in the plant data are due to perturbations occurring in the feed streams (catalyst, hydrogen, and ethylene). Fig. 7 shows also that the ethylene consumption increases rapidly with an increase of the catalyst feed rate, leading to a pronounced increase of the hydrogen/ethylene ratio in the reactor gas phase.

The advantages of the orthogonal collocation technique as a tool to solve the equations of the multigrain model should be adequately stressed. Table 8 compares the computational time for the simulation of 1500 min of reactor operation time using two different types of numerical procedures, the finite difference method with 25 shells (Hutchinson [11]) and the orthogonal collocation technique with 5 interior points (the model included only one type of site). As it is observed, the dimension of the numerical models, and consequently the computational

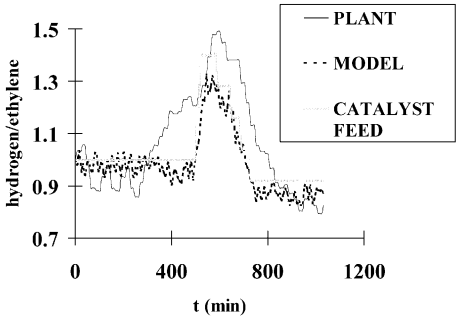

Fig. 7. Normalized hydrogen/ethylene ratio for an operational run.

Table 8
Solution of the dynamic model.

Discretization method for multigrain equations	Number of ODE's	Simulation time, min
Finite difference (25 shells)	608	134
Orthogonal collocation (5interior points)	153	9

times, were quite different, with an expressive advantage for the use of the orthogonal collocation technique.

6. Conclusions

The complex nature of slurry polymerization systems, related to the existence of different types of mechanisms actuating simultaneously at different scales, was handled in the present work by the use of a methodology that integrated the results at the micro and meso scales directly with the macroscopic balances for the reactor. The multigrain model was used at the meso scale together with comprehensive local balances for the reactive species and for the moments, while the kinetic model included the existence of two types of catalytic sites. The dynamic model of the reactor accounts for the effects of the different inputs.

The simulation of the reactor model made use of the orthogonal collocation technique to solve the multigrain model. A small number of interior collocation points was enough to provide a satisfactory description of the process dynamics, thus leading to an expressive reduction of the computational effort.

The results are qualitatively consistent with the expected behavior for the process variables and polymer properties. The hydrogen/ethylene ratio predictions follow the dominant tendency of plant data, even without the existence of measurements of hydrogen feed flow that has a pronounced effect in this case.

Acknowledgements

The authors acknowledge the financial support provided by CNPq through a grant to C. Fontes as well as the technical support from Polialden S.A.

Appendix A. Appendix

Let $\bar{\Gamma}_{n,m}$ be the mean concentration (mol/unit volume catalyst) of an entity associated exclusively to the macroparticle, like, for example, $P_{\mathrm{j}}(0,0)$, $P_{1j}(\mathrm{n,m})$, $\lambda_j^{n,m}$… The macroscopic balance for such entity is:

$$\frac{\mathrm{d}[\bar{\Gamma}_{n,m}(t)V_{\mathrm{c}}(t)]}{\mathrm{d}t} = \bar{\Gamma}^{o}_{n,m}(t)\dot{V}_{\mathrm{ce}} + \bar{R}_{\Gamma_{n,m}}(t)V_c(t) - \bar{\Gamma}_{n,m}(t)\dot{V}_{\mathrm{cs}} \tag{A1}$$

where V_{c} is the volume of catalyst in reactor, $\dot{V}_{\mathrm{ce}}$ and $\dot{V}_{\mathrm{cs}}$ are respectively the flow rates of catalyst entering and leaving the reactor, $\bar{R}_{\Gamma_{n,m}}$ is the mean rate of production of $\Gamma_{n,m}$ (per unit volume of catalyst), and $\Gamma^{o}_{n,m}$ is the value of $\Gamma_{\mathrm{n,m}}$ in the catalyst entering the reactor.

With the macroscopic balance for the catalyst

$$\frac{\mathrm{d}V_{\mathrm{c}}(t) = \dot{V}_{\mathrm{ce}} - \dot{V}_{\mathrm{cs}},}{\mathrm{d}t} \tag{A2}$$

becomes

$$\frac{\mathrm{d}\bar{\Gamma}_{n,m}(t)}{\mathrm{d}t} = \bar{R}_{\Gamma_{n,m}}(t) + (\bar{\Gamma}^{o}_{n,m}(t) - \bar{\Gamma}_{n,m}(t))\frac{\dot{V}_{\mathrm{ce}}}{V_{\mathrm{c}}(t)} \tag{A3}$$

The mean variables $\bar{R}_{\Gamma_{n,m}}$ and $\bar{\Gamma}_{n,m}$ are related to its local values inside the macroparticles by

$$\bar{R}_{\Gamma_{n,m}} = \frac{\int_{V_{\mathrm{m}}} R_{\Gamma_{n,m}}(r,t)[(1-\varepsilon)\phi^3]\mathrm{d}V_{\mathrm{m}}}{\int_{V_{\mathrm{m}}}[(1-\varepsilon)\phi^3]\mathrm{d}V_{\mathrm{m}}} \tag{A4}$$

and

$$\bar{\Gamma}_{n,m}(t) = \frac{\int_{V_{\mathrm{m}}} \Gamma_{n,m}(r,t)[(1-\varepsilon)\phi^3]\mathrm{d}V_{\mathrm{m}}}{\int_{V_{\mathrm{m}}}[(1-\varepsilon)\phi^3]\mathrm{d}V_{\mathrm{m}}} \tag{A5}$$

where

$$R_{\Gamma}(r,t)\sum_{j=1}^{2} R^{i}_{\Gamma}(r,t), \quad \Gamma(r,t)\sum_{j=1}^{2}\Gamma_j(r,t).$$

But,

$$\int_{V^{o}_{\mathrm{m}}}[(1-\varepsilon)/\phi^3]\mathrm{d}V^{o}_{\mathrm{m}} = \int_{V_{\mathrm{m}}}[(1-\varepsilon)/\phi^3]\mathrm{d}V_{\mathrm{m}}. \tag{A6}$$

Because the volume of catalyst in the macroparticle is constant. As there is no flow of $\Gamma_{n,m}$ through the surface of the macroparticle, and the initial distribution $\Gamma^{o}_{n,m}$ may be considered uniform, one obtains, from equations (A3)–(A5):

$$\int_{V_{\mathrm{m}}}\frac{\partial\Gamma_{n,m}(r,t)}{\partial t}[(1-\varepsilon)/\phi^3]\mathrm{d}V_{\mathrm{m}} = \int_{V_{\mathrm{m}}} R_{\Gamma_{n,m}}(r,t)[(1-\varepsilon)/\phi^3]\mathrm{d}V + \frac{\dot{V}_{\mathrm{ce}}}{V_{\mathrm{c}}(t)}\left[\int_{V_{\mathrm{m}}}\Gamma^{o}_{n,m}[(1-\varepsilon)/\phi^3]\mathrm{d}V_{\mathrm{m}} - \int_{V_{\mathrm{m}}}\Gamma_{n,m}(r,t)[(1-\varepsilon)/\phi^3]\mathrm{d}V_{\mathrm{m}}\right],$$

or, finally

$$\frac{\partial \Gamma_{n,m}(r,t)}{\partial t} = R_{\Gamma_{n,m}}(r,t) + \left[\Gamma^{o}_{n,m} - \Gamma_{n,m}(r,t)\right]\frac{\dot{V}_{ce}}{V_c(t)} \qquad \text{(A7)}$$

References

[1] Schnelle P, Rollins DL. ISA Trans 1998;36:281.
[2] Rawlings JB. In: Proceedings of the American control conference; San Diego, California, 1999. p. 662.
[3] Ray WH. Ber Bunsenges Phys Chem 1986;90:947.
[4] Kiparissides C. Chem Eng Sci 1996;51:1637.
[5] Dube MA, Soares JBP, Penlidis A, Hamielec AE. Ind Eng Chem Res 1997;36:966.
[6] Soares JBP, Hamielec AE. Polym React Eng 1995;3:261.
[7] Floyd S, Heiskanen T, Ray WH. Chem Eng Prog 1988;56.
[8] McKenna TF, Soares JBP. Chem Eng Sci 2001;56:3931.
[9] Aris R. Elementary chemical reactor analysis. New Jersey: Prentice-Hall; 1969.
[10] Ray WH. J Macromol Sci, Revs Macromol Chem 1972;C8:1.
[11] Hutchinson RA, Chen CM, Ray WH. J Appl Polym Sci 1992;44:1389.
[12] Fontes CH. PhD Thesis, Unicamp, Campinas, Brazil; 2001.
[13] Floyd S, Choi KY, Taylor TW, Ray WH. J Appl Polym Sci 1986;32: 2935.
[14] Soares JBP, Hamielec AE. Polym React Eng 1996;4:153.
[15] Zacca JJ, Debling JA, Ray WH. Chem Eng Sci 1996;51:4859.
[16] Galvan R, Tirrell M. Comput Chem Eng 1986;10:77.
[17] Freitas M. D.Sc. Thesis, Universidade Federal do Rio de Janeiro, Rio de Janeiro, Brazil; 1998.
[18] Marrone GM, Kirwan DJ. AIChE Journal 1986;32:523.
[19] McAuley KB, MacGregor JF, Hamielec AE. AIChE Journal 1990;36: 837.
[20] McKenna TF, Dupuy J, Spitz R. J Appl Polym Sci 1995;57:371.
[21] Sun J, Eberstein C, Reichert K. J Appl Polym Sci 1997;64:203.
[22] Villadsen J, Michelsen ML. Solution of differential equation models by polynomial approximation. Englewood Cliffs: Prentice-Hall; 1978.
[23] Le Roux GC. PhD Thesis, Institut National Polytechnique de Toulouse; 1995.
[24] Moudgalya KM, Jaguste S. Chem Eng Sci 2001;56:3611.
[25] Qin SJ, Badgwell TA. In: Allgöwer F, Zheng A, editors. Nonlinear model predictive control. Progress in systems and control theory series, vol. 26. Switzerland: Birkhauser Boston; 2000.
[26] Ozkan G, Ozen S, Ergogan S, Hapoglu H, Alpbaz M. Comput Chem Eng 2001;25:757–63.